Self-consistent mapping: Effect of local environment on formation of magnetic moment in α-FeSi₂

V. S. Zhandun,[*] N. G. Zamkova, S. G. Ovchinnikov, and I. S. Sandalov

Kirensky Institute of Physics, Federal Research Center "Krasnoyarsk Science Centre, Siberian Branch of the Russian Academy of Sciences",
660036 Krasnoyarsk, Russia

The Hohenberg-Kohn theorem establishes a basis for mapping the exact energy functional to a model one provided that their charge densities coincide. We suggest to use a mapping in a similar spirit, but here the parameters of the formulated multiorbital model should minimize the difference between the self-consistent charge and spin densities. The analysis of the model allows for detailed understanding of the role played by different parameters of the model in the physics of interest. After finding the areas of interest in the phase diagram of the model, we return to the *ab initio* calculations and check if the effects discovered are confirmed or not. Because of the last controlling step, we call this approach hybrid self-consistent mapping approach (HSCMA). As an example of the approach we present a study of the effect of silicon atoms substitution by the iron atoms and vice versa on the magnetic properties in the iron silicide α-FeSi₂. We find that while the stoichiometric α-FeSi₂ is nonmagnetic, the substitutions generate different magnetic structures depending on the type of local environment of the substitutional Fe atoms. Besides, contrary to the commonly accepted statement that the destruction of the magnetic moment is controlled only by the number of Fe-Si nearest neighbors, we find that actually it is controlled by the Fe-Fe *next*-nearest-neighbor hopping parameter. This finding led us to the counterintuitive conclusion: an *increase of Si concentration* in $Fe_{1-x}Si_{2+x}$ ordered alloys may lead to ferromagnetism. The calculation within GGA-to-DFT confirms this conclusion.

I. INTRODUCTION

A method of mapping first-principles density functional theory (DFT) calculations to an effective Heisenberg model for the theoretical study of the magnetic properties of solids was developed in a series of works [1]. The role played by the electronic subsystem in this approach is reduced to the formation of the lowest-order pairwise effective exchange interaction of classical spins. In order to have an opportunity to use the well-developed many-body perturbation theory and to obtain a physical picture of the formation of the magnetic and, especially, the nonmagnetic properties of the matter by the electronic subsystem, one either has to use Hedin's GW approximation [2] or a detailed model that includes all atoms, their key orbitals, the symmetry of the lattice in question, hopping parameters, and Coulomb interactions. The GW approximation (even without the vertex corrections) is extremely time and computer-resources consuming. For this reason, the route with more simple model Hamiltonians seems to be more efficient for highlighting the physics. Besides, an application of LDA-to-DFT approach is also restricted. Since the exact form of the exchange-correlation functional Φ_{xc} is unknown, a big variety of $\tilde{\Phi}_{xc}$ has been suggested. Unfortunately, the complexity of the strict equation [3,4] for the exchange-correlation potential prevents the derivation of these approximate functionals $\tilde{\Phi}_{xc}$ (except of the simple cases discussed in Ref. [4]); the small parameter of the theory is unknown or absent. For this reason and due to the nonlinearity of the problem, it is very difficult to construct a regular perturbation theory for an analysis of the reasons, why this or that functional $\tilde{\Phi}_{xc}$ does not work for the description of some materials or properties. Nevertheless, LDA-based

calculations often give a remarkably good description of the ground-state properties. Therefore a model, which would (i) allow us to use a regular perturbation theory and (ii) be able to describe the same material with an accuracy reasonably close to the one obtained within an *ab initio* calculation, is highly desirable indeed. There exist also other reasons for constructing realistic models. In spite of the fact that the Hohenberg-Kohn theorem provides a solid ground for the description of the ground-state properties only, namely, the full energy and the charge density, the intermediate-step *auxiliary* Kohn-Sham bands very often are used for the interpretation of phenomena that arise due to excitations. Although sometimes this leads to results that describe experiment, the theoretical grounds for it remain unclear. An investigation of excitations within a model approach does not create such questions.

A use of a model, however, raises the question: to what extent this or that model is applicable for the description of a concrete material? In general, each model has its phase diagram in the multidimensional space of its parameters, even for an adequate model and approximation.

Probably, only one point in this multidimensional parameter space of the model corresponds to each real material. The largest parameters of a model intended for the description of d or f materials are intratomic interactions. A change of the external conditions for the material, such as applying a pressure, changing the temperature, or placing a film of the material on some substrate, involves energies of a much smaller scale. Therefore these changes will move the point from the initial position only slightly.

So, a principle is needed for finding this region. We suggest that the requirement that the charge densities obtained in these two approaches should be as close to each other as possible can be taken as an underlying principle. The principle of equality of the model $\rho[x; v_{xc}]$ and "genuine" $\rho[x; \Sigma]$ charge densities has been used by Sham and Schlüter for the derivation of

---

*jvc@iph.krasn.ru

the equation for the calculation of the exchange-correlation potential v_{xc} via the known self-energy Σ (see Ref. [4], Eq. (10); in the form adopted for the case of atomic-orbital basis, set see Ref. [5], Eq. (41)). In the symbolic form, this equation is (x is a real-space coordinate):

$$\rho[x; \Sigma] = \rho[x; v_{xc}]. \tag{1}$$

Unfortunately, it is not known which approximation has to be used for the self-energy Σ of the single-electron Green's function G in order to reproduce even the routinely used exchange-correlation potentials v_{xc}. The calculations of v_{xc} for the approximate expressions for the self-energy Σ also are not known (except discussed in Ref. [4]). For this reason, we suggest to use an alternative route. We can take an expression for the self-energy $\Sigma(A)$ calculated for the model with the set of the parameters A and try to use this set as fitting parameters. They can be found, e.g., from the minimization of the function

$$\Upsilon(x; A) = (\rho[x; \Sigma(A)] - \rho[x; v_{xc}])^2. \tag{2}$$

This step distinguishes our approach from those suggested earlier [1,6,7]. The construction of the hopping parameters for certain symmetries has been described by Slater and Koster [8].

Then, having obtained some prediction within the model calculations, we return to the first-principles ones in order to check the validity of the model prediction. This is the essence of the suggested here hybrid self-consistent mapping approach (HSCMA). It may seem that such an approach should work only within the validity domain of the chosen approximation for the DFT (in our case, GGA-to-DFT approximation). However, the largest contribution to the energy of the system and the formation of the local charge density $\rho_{DFT}(r)$ comes from the Hartree part of the interaction, which is treated in DFT pretty well. That is why we want to start *at least* from a point in the model parameter space that provides $\rho_{model}(r)$ close to $\rho_{DFT}(r)$. Further, the model with these parameters can be used for studying phenomena beyond the reach of DFT, e.g., collective excitations, or temperature effects. Then the question arises why we require that, namely, that the *self-consistent* charge densities (magnetic moments) in the model and DFT should be close to each other?

The matter is that we want to know the *bare* parameters of the model in order to be able to use the diagrammatic methods for dressing them and to avoid the double-counting problem. This approach is attractive also because it does not take any fitting parameters from experiment and, therefore, can be considered as a first-principles approach.

The HSCMA is applied here for the analysis of the magnetic properties of α-FeSi$_2$–based ordered alloys. The ferromagnet/semiconductor/ferromagnet nanostructures attracted much attention soon after the discovery of the giant magnetoresistivity in the ferromagnet/nonmagnetic-metal/ferromagnet structures by A. Fert and P. Grunberg. The idea to use a semiconducting spacer instead of a metallic one is potentially very appealing for spintronics. Silicon is the most used semiconductor, so Fe/Si/Fe epitaxial structures reveal a strong antiferromagnetic interlayer coupling and its interplay with the transport properties has been studied by a number of groups. A very important difference with metallic spacers is the formation of a variety of Fe-Si phases in the interface [9–12]. To this day, several iron-silicide structures have been reported. At the Fe-rich side

of the binary phase diagram, metallic as well as ferromagnetic Fe$_3$Si (DO$_3$ structure) [13,14] have already been established. An unknown metallic, ferromagnetic at room temperature phase, Fe$_5$Si$_3$, has been recently obtained in the form of a nanowire [15] and thin film [15]. The Si-rich side of the phase diagram contains several variants of a disilicide stoichiometric compound, such as the high-temperature tetragonal metallic α-FeSi$_2$ phase [16], with applications as an electrode or an interconnect material [17,18], and the orthorhombic semiconducting β-FeSi$_2$ phase [19], which due to its direct band gap is an interesting candidate for thermoelectric, photovoltaic, and optoelectronic devices [20]. While the room-temperature stable β phase is well-studied, the tetragonal α phase did not attract great interest until recently. This is because this phase is metastable and exists only at temperatures above $950\,^{\circ}\text{C}$ [16]. However, the iron silicides, which do not exist in bulk, can be stabilized as films. In Refs. [17,21–24], a successful fabrication of thin films α-FeSi$_2$ was reported. Also, while the magnetic order is not observed in bulk stoichiometric disilicide α-FeSi$_2$, ferromagnetism was found [24] in the metastable phase α-FeSi$_2$, which was stabilized in an epitaxial film grown on a silicon substrate. The authors of Refs. [18,25] reported the magnetic moments of Fe atoms in α-FeSi$_2$ nanoislands and nanostripes on a Si (111) substrate to be $\mu = 1.8\mu_B$ [18] and $\mu = 3.3\mu_B$, respectively [25]. These experimental achievements offered a good prospect for the integration of FeSi-based magnetic devices into silicon technology, and, therefore, demand a detailed understanding of the physics of the magnetic moment formation in these compounds.

Traditionally, the appearance of the magnetic structure in Fe-Si alloys is related to the increase of the concentration of Fe atoms. So, the authors of Ref. [24] explain the unusual ferromagnetism in the epitaxial film α-FeSi$_2$ by the appearance of substitutional Fe atoms on the Si sublattice. According to the *ab initio* calculation in the framework of the coherent potential approximation (CPA) performed in Ref. [24], the ferromagnetism in thin films α-FeSi$_2$ appears with the substitution of a small percent of silicon atoms by iron atoms. Particularly, when the concentration of substitution Fe atoms reaches 3.3%, these Fe atoms acquire a magnetic moment $\mu = 2.4\mu_B$. A similar explanation of anomalously high total magnetic moment was suggested also by the authors of Refs. [18,25]. A decrease of the magnetic moments of Fe atoms with the increase of the Si concentration was observed experimentally in the iron silicides Fe$_x$Si$_{1+x}$ and discussed in the framework of the phenomenological local environment models [26–28]. It was noticed that the change of the magnetic moments of Fe atoms in iron silicides, Fe$_x$Si$_{1+x}$, rather depends on the number of Si atoms in the nearest local environment of iron and not on the concentration of Si atoms. In our work [29], the mechanism of magnetic moment formation in Fe$_3$Si is analyzed in the framework of the multiorbital model, where it is shown that the neighboring Fe atoms along crystallographic axes as well as Si atoms in the first coordination sphere play the crucial role in the destruction of the Fe magnetic moments. Namely, the increase of the number of such Fe neighbors leads to the decrease of the Fe magnetic moment. Iron atoms in α-FeSi$_2$ have only silicon atoms as the nearest neighbors and from the traditional point of view [26–28], it is naturally to assume that the absence of the magnetism in this silicide is caused by
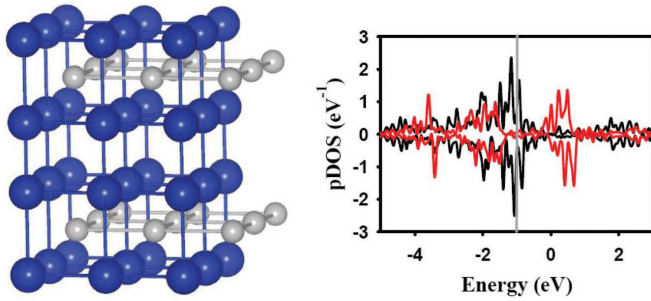
FIG. 1. (Left) Structure of α-FeSi$_2$; Si atoms are shown by blue balls, Fe atoms shown by grey balls. (Right) Partial density of electronic states (pDOS) of Fe atoms; black line shows t_{2g} states, red line shows e_g states. The zero on the energy axis is chosen at the Fermi energy.

the nearest silicon environment. However, the specific feature of the α-FeSi$_2$ structure is the presence of alternating Fe and Si planes, which are perpendicular to the tetragonal axis of the cell [Fig. 1(a)]. In such a plane, Fe atoms are surrounded only by Fe atoms arranged along the crystallographic axes. Our analysis [29] prompts that such mutual arrangement of Fe atoms should result in a magnetic moment destruction. The target of this work is to investigate the influence of the local environment on the formation of the magnetic moments on iron atoms in the silicide α-FeSi$_2$, its ordered Fe-rich solid solutions with substitutional Fe atoms, Fe$_{1+x}$Si$_{2-x}$, and Si-rich ones with substitutional Si atoms, Fe$_{1-x}$Si$_{2+x}$. Particularly, we will address the question about the role played by second neighbors of Fe ions in the physics of magnetic moment formation.

The paper is organized as follows. In Sec. II, we provide the details of *ab initio* and model calculations. The results of the *ab initio* calculations of α-FeSi$_2$ and its Fe-rich alloys are given in Sec. III A. The results of the model calculations of α-FeSi$_2$ and its Fe-rich alloys and the dependence of magnetic moments on the hopping matrix elements are presented in Sec. III B. The results of the *ab initio* investigation of Si-rich alloys of α-FeSi$_2$ are described in Sec. III C. Section IV contains the summary of the obtained results and conclusions.

II. HSCMA: THE HYBRID *AB INITIO* AND MODEL CALCULATION METHOD

In this work, we combine the *ab initio* calculations with the model ones. The arguments that forced us to turn to the models are the following.

We use the following scheme. First, we perform a calculation of the electronic and magnetic properties of the compound of interest within the framework of DFT-GGA for different ways of silicon atom substitution by iron atoms taking into account the relaxation of atomic positions. Then we map the DFT-GGA results onto the multiorbital model, suggested in Ref. [29]. The guiding arguments for the formulation of the model are the following: the model should (1) contain as little as possible parameters; (2) contain the specific information about the compound in question, i.e., contain a proper number of orbitals and electrons, and to possess the symmetry of the corresponding crystal structure, and (3) contain the main interactions, reflecting our understanding of the underlying physics.

The details of the model calculation are described in Ref. [29]. We use the set of Kanamori interactions [30] between the d electrons of Fe (5d orbitals per spin). The structure contains neighboring Fe ions, for this reason the interatomic direct d-d exchange and d-d hopping are included too. The Si p electrons (3p orbitals per spin) are modeled by atomic levels and interatomic hoppings. Both subsystems are connected by d-p hoppings. Thus the Hamiltonian of the model is

$$H = H^{\text{Fe}} + H_{J'}^{\text{Fe-Fe}} + H_0^{\text{Si}} + H_{\text{hop}}, \qquad (3)$$

where

$$H^{\text{Fe}} = H_0^{\text{Fe}} + H_K^{\text{Fe}},$$
$$H_0^{\text{Fe}} = \sum \varepsilon_0^{\text{Fe}} \hat{n}_{nm\sigma}^d,$$
$$H_0^{\text{Si}} = \sum \varepsilon_0^{\text{Si}} \hat{n}_{nm\sigma}^p;$$

and the Kanamori' s part of the Hamiltonian

$$H_K^{\text{Fe}} = \frac{U}{2} \sum \hat{n}_{nm\sigma}^d \hat{n}_{nm\bar{\sigma}}^d + \left(U' - \frac{1}{2}J \right)$$
$$\times \sum \hat{n}_{nm}^d \hat{n}_{nm'}^d (1 - \delta_{mm'}) - \frac{1}{2}J \sum \hat{s}_{nm}^d \hat{s}_{nm'}^d,$$

$$H_{J'}^{\text{Fe-Fe}} = -\frac{1}{2}J' \sum \hat{s}_{nm}^d \hat{s}_{n'm'}^d,$$

$$H_{\text{hop}} = \sum T_{n,n'}^{mm'} p_{nm\sigma}^\dagger p_{n'm'\sigma} + \sum t_{n,n'}^{mm'} d_{nm\sigma}^\dagger d_{n'm'\sigma}$$
$$+ \sum \left[(t')_{n,n'}^{mm'} d_{nm\sigma}^\dagger p_{n'm'\sigma} + \text{H.c.} \right],$$

$$\hat{n}_{nm\sigma}^d \equiv d_{nm\sigma}^\dagger d_{nm\sigma}; \quad \hat{n}_{nm}^d = \hat{n}_{nm\uparrow}^d + \hat{n}_{nm\downarrow}^d;$$

$$\hat{s}_{nm}^d \equiv \boldsymbol{\sigma}_{\alpha\gamma} d_{nm\alpha}^\dagger d_{nm\gamma}; \quad \hat{n}_{nm\sigma}^p \equiv p_{nm\sigma}^\dagger p_{nm\sigma}. \qquad (4)$$

Here, $p_{nm\sigma}^\dagger (p_{nm\sigma})$ and $d_{nm\sigma}^\dagger (d_{nm\sigma})$ are the creation (annihilation) operators of p electrons on Si and d electrons on Fe ions; n is a complex lattice index, (site, basis); m labels the orbitals; σ is the spin projection index; $\boldsymbol{\sigma}_{\alpha\gamma}$ are the Pauli matrices; U, $U' = U - 2J$, and J are the intra-atomic Kanamori parameters; J' is the parameter of the intersite exchange between nearest Fe atoms. At last, $T_{n,n'}^{mm'}$, $t_{n,n'}^{mm'} (t')_{n,n'}^{mm'}$ are hopping integrals between Si-Si, Fe-Fe, and Fe-Si atoms, correspondingly. The dependencies of hopping integrals $T_{n,n'}^{mm'}$, $t_{n,n'}^{mm'} (t')_{n,n'}^{mm'}$ of **k** were obtained from the Slater and Koster atomic orbital scheme [8] in the two-center approximation using a basic set consisting of five $3d$ orbitals for each spin on each Fe and three $3p$ orbital for each spin on each Si. In this two-center approximation, the hopping integrals depend on the distance $\mathbf{R} = (l\mathbf{x} + m\mathbf{y} + n\mathbf{z})$ between the two atoms, where **x**, **y**, and **z** are the unit vectors along the cubic axes and l, m, and n are direction cosines. Then, within the two-center approximation, the hopping integrals are expressed in terms of Slater-Koster parameters $t_\sigma = (dd\sigma)$, $t_\pi = (dd\pi)$, and $t_\delta = (dd\delta)$ for Fe-Fe hopping, $t_\sigma = (pd\sigma)$, $t_\pi = (pd\pi)$ for Fe-Si, and $t_\sigma = (pp\sigma)$, $t_\pi = (pp\pi)$ for Si-Si hoppings (σ, π, δ specifies the components of the angular momentum relative to the direction $\mathbf{R}$). Their **k** dependence is given by the functions $\gamma_\sigma(\mathbf{k})$, $\gamma_\pi(\mathbf{k})$, and $\gamma_\delta(\mathbf{k})$, where $\gamma(\mathbf{k}) = \sum_{\mathbf{R}} e^{i\mathbf{k}\mathbf{R}}$. The expressions for hopping integrals can be obtained from Table I in Ref. [8]. For example, $t_{\text{Fe-Fe}}^{xy,xy}(\mathbf{k}) = 2t_\pi [\cos(R_x k_x) + \cos(R_y k_y)] + 2t_\delta \cos(R_z k_z),$

etc. The number of points in the Brillouin zone was taken to be 1000. The Monkhorst-Pack scheme [31] was used for generation of the k mesh. The model is solved within the Hartree-Fock approximation (HFA). The band structure arises due to hopping parameters, which connect nearest neighbors (NN) and next NN (NNN) sites. The calculations were performed for three initial states: ferromagnetic (FM), antiferromagnetic (AFM), and paramagnetic (PM) states. After achieving self-consistency, the state with minimal total energy was chosen. The last step was done with the help of the Galitsky-Migdal formula for total energy (Eq. (10) in Ref. [29]), which we adopted for our model. For the model used here, the set of fitting parameters in Eq. (2) is $A = t, t', T, U, U', J$, and J'. Both charge (and spin) densities together with the self-energy have to be found self-consistently for each set of fitting parameters. Since the model Hamiltonian misses a lot of interactions compared to the ones taken into account in the corresponding density functional theory (DFT), one cannot expect that the model will fully reproduce all the details of the charge density, density of states, and so on.

In order to decrease the complexity of Eq. (2), which comes from the necessity to find the self-consistent solution for $\rho[x; \Sigma(A)]$ for each set of parameters A, we simplified Eq. (2) further: instead of minimization of the function $\Upsilon(x, A)$ with respect to the differences of the electron spin density in each point of space, we have fitted the number of d electrons n_f^d, the magnetic moments m_f^d and the partial d densities of states for each type f of Fe atom:

$$\Upsilon(A) = \sum_f \left(n_f^d[\Sigma(A) - n_f^d[v_{xc}] \right)^2$$
$$+ \sum_f \left(m_f^d[\Sigma(A) - m_f^d[v_{xc}] \right)^2$$
$$+ \int dE \sum_f \left(g_f^{(mod)}(E) - g_f^{(LDA)}(E) \right)^2. \quad (5)$$

After that, the predictions of the model have been tested within the DFT-based calculation. All *ab initio* calculations presented in this paper have been performed using the Vienna *ab initio* simulation package (VASP) [32] with projector augmented wave (PAW) pseudopotentials [33]. The valence electron configurations $3d^6 4s^2$ are taken for Fe atoms and $3s^2 3p^2$ for Si atoms. The calculations are based on the density functional theory where the exchange-correlation functional is chosen within the Perdew-Burke-Ernzerhoff (PBE) parametrization [34] and the generalized gradient approximation (GGA) has been used. Throughout all calculations, the plane-wave cutoff energy is 500 eV and the Gauss broadening with smearing 0.05 eV is used. The Brillouin-zone integration is performed on the grid Monkhorst-Pack [31] special points $8 \times 8 \times 6$. The optimized lattice parameters and atom coordinates were obtained by minimizing the full energy.

III. RESULTS AND DISCUSSION

A. *Ab initio* calculations

The stoichiometric compound α-FeSi$_2$ has tetragonal space symmetry group $P4/mmm$ with one formula unit per cell. The
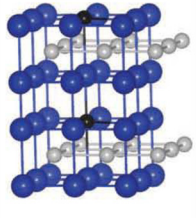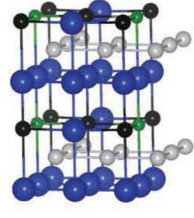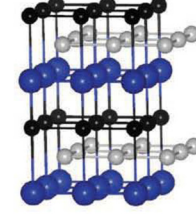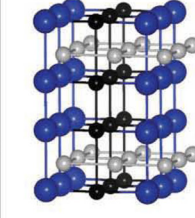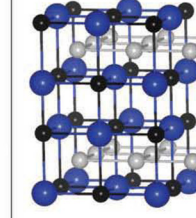
structure is shown in Fig. 1(a). The compound is a nonmagnetic metal with lattice parameters from our *ab initio* calculations $a = 2.70$ Å and $c = 5.13$ Å, which are in a good agreement with the experimental values [35]. The structure of α-FeSi$_2$ consists of alternating planes of iron and silicon atoms Fe-Si-Si-Fe, which are perpendicular to the tetragonal axis of the cell. Iron atoms are surrounded by eight silicon atoms ($R_{Fe-Si} = 2.36$Å) located in the corners of a slightly distorted in the [001] direction cube, the next nearest neighbors (NNN) of iron atoms are Fe atoms arranged along crystallographic axes x and y, forming the iron plane ($R_{Fe-Fe} = 2.70$ Å). The full density of states of α-FeSi$_2$ was calculated in the works [36–38] and in our recent work [39], thus, in the present paper, we give only the partial spin-projected density (pDOS) of Fe d-electron states in Fig. 1(b). As seen, both t_{2g} and e_g electrons are delocalized in a wide energy range and magnetism is absent.

However, as was mentioned in Introduction, several recent studies [18,24,25] discovered that a ferromagnetic state arises in the films of α-FeSi$_2$. The explanation of the emergence of the magnetic structure, suggested in these works, is within the commonly accepted opinion that the magnetism arises due to an increase of Fe concentration in the material. The used theoretical approaches, CPA in Ref. [24] and phenomenological local environment models in Refs. [18,25], take into account, however, only a part of the local environment effects because a full account of them is beyond the reach of the standard CPA methods by construction, whereas the local environment models [26,27] take into account the nearest environment only. In Ref. [29], we found that the next-nearest-neighbor environment (NNN) plays a crucial role in the magnetic moment formation. This motivates us to include the NNN local environment effects into the study of the magnetic properties of Fe-rich ordered alloys both in the framework of DFT calculations and the subsequent analysis in the suggested multiorbital model too. The different local environment of iron atoms was set by the different spatial arrangement and number of substitutional Fe atoms in the ordered alloys Fe$_{1+x}$Si$_{2-x}$. In this part of paper, we presented the results of our *ab initio* calculations of some of ordered alloys Fe$_{1+x}$Si$_{2-x}$. We used for the calculations the supercell $2a \times 2a \times c$, where a and c are the lattice parameters of stoichiometric α-FeSi$_2$.

The ordered alloys considered in the present work are shown in Table I. Alloys A and B contain one and three substitutional Fe atoms at the Si sites in the Si planes, correspondingly. In the last three alloys C, D, and E, four Si atoms were replaced by Fe atoms in different ways: in the plane perpendicular to c axis (C), in the plane parallel to c axis (D) и chess-mate replacement (E). The lattice parameters and calculated magnetic moments on the host iron atoms in Fe sublattice of α-FeSi$_2$ (Fe$_0$) and on the substitutional iron atoms (Fe$_I$ and Fe$_{II}$) obtained after full optimization of geometry are given in Table I. The geometry optimization results in the elongation of all cells along c axis and to the compression in the (ab) plane, which are most pronounced for the C and E alloys.

The substitution of one Si atom by iron (A) results in the appearance of large magnetic moments [$\mu(Fe_I) = 2.7\mu_B$] on the substitutional Fe$_I$ atom. Although the alloy A is ordered, the obtained result coincides with the result obtained in CPA [24] for a random alloy. The value of the magnetic moment

TABLE I. The structures of some of ordered alloys, the optimized lattice parameters and the calculated magnetic moments; the colors encode Si atoms by blue, host Fe_0 atoms by grey, and the substitutional Fe_I and Fe_{II} atoms by black and green, correspondingly.

A	B	C	D	E
$a=b=5.37$ Å $c=5.22$ Å	$a=b=5.23$ Å $c=5.37$Å	$a=b=5.05$ Å $c=5.22$ Å	$a=5.15$Å $b=5.37$ Å $c=5.37$Å	$a=b=4.80$ Å $c=6.13$Å
$\mu(Fe_0)=0.2\,\mu_B$	$\mu(Fe_0)=0.5\,\mu_B$	$\mu(Fe_0)=0.0\,\mu_B$	$\mu(Fe_0)=1.5\,\mu_B$	$\mu(Fe_0)=2.0\,\mu_B$
$\mu(Fe_I)=2.7\,\mu_B$	$\mu(Fe_I)=2.6\,\mu_B$	$\mu(Fe_I)=0.0\,\mu_B$	$\mu(Fe_I)=2.5\,\mu_B$	$\mu(Fe_I)=1.3\,\mu_B$
	$\mu(Fe_{II})=-2.1\,\mu_B$			

and pDOS on the substitutional Fe atom are in good agreement with the ones from Ref. [24]. The general feature of both DOS is the sharp peak at the energy ~ -3 eV, which originates from the minority t_{2g} state of d electrons (Fig. 2).

A further increase of substitutional Fe concentration leads to nontrivial results that clearly illustrate the dependence of Fe magnetic moments on the local environment. As seen from Table I, the substitution of three Si atoms by Fe ones (alloy B) results in the appearance of the ferri magnetic state: the substitutional Fe_I and Fe_{II} atoms become inequivalent, they acquire large magnetic moments, which are not equal to each other, and directed into opposite directions. The absolute values of magnetic moments are close to the ones in alloy A. Alloy B presents only one of the possible ways to order three substitutional Fe atoms in the supercell. Other nonequivalent orderings of the substitutional Fe atoms are shown in Table II. Our *ab initio* calculations show that the type of the magnetic structure, ferrimagnetic or ferromagnetic, is determined by the spatial arrangement of substitutional Fe atoms. Indeed, the first two alloys in Table II are ferrimagnetic, and the last three are ferromagnetic. The same dependence of the iron magnetic moments on the spatial arrangement (and hence on the local

environment) arises for the alloys with four substitutional Fe atoms on Si sites (C, D, and E in Table I). The alloy C and α-FeSi$_2$ are nonmagnetic, while the magnetic moments in alloys D and E appear on the substitutional Fe_I and on the host Fe_0 atoms. The pDOSs of substitutional Fe_I in alloys B, D, and E are similar to the ones in alloy A, the pDOS of Fe_{II} in alloy B atom is mirror-symmetric to pDOS of Fe_I. Notice that the t_{2g} states form a peak in pDOS of the substitutional Fe_I atom when the latter has a magnetic moment while the pDOS of Fe_I d electrons in the nonmagnetic alloy C is similar to the one for the Fe atom in α-FeSi$_2$ (Fig. 1 b): t_{2g} and e_g electron states are delocalized in a wide energy range.

Thus our *ab initio* calculations confirm only part of the conclusions, derived from the local environment models [26,27]: ferromagnetism arises with an increase of the Fe concentration indeed, but the types of the magnetic structure of the ordered Fe$_{1+x}$Si$_{2-x}$ alloys that we obtain are essentially different even at the same concentration of substitutional Fe atoms (Tables I and II)—the magnetic moments on Fe atoms are determined by the composition and the configuration of its local environment. These findings motivate us to investigate the role played by the different local environments on the magnetic moment formation in Fe-Si alloys, more carefully in the framework of the multiorbital model suggested in Ref. [29] and briefly outlined in Sec. II. As was pointed out in Ref. [29], the crucial role in the magnetic structure formation in iron silicides is played by both nearest and next-nearest local environment. Both are taken into account in a model calculation.

$\mu(Fe_0)=0.2\mu_B$ $\mu(Fe_I)=2.7\mu_B$

FIG. 2. pDOS for host Fe_0 (left) and substitutional Fe_I (right) in alloy A. Black line shows t_{2g} states and red line shows e_g states. The zero on the energy axis is the Fermi energy.

B. The model calculations

In this section, we describe the results of our model calculations for the stochiometric α-FeSi$_2$ and its ordered Fe-rich alloys Fe$_{1+x}$Si$_{2-x}$(B, C, and D in Table I). The hopping matrix elements fully reflect the crystal symmetry and split the atomic states of Fe ions according to the symmetry of the local environment. For this reason, we decreased the number of fitting parameters in the model calculations and kept
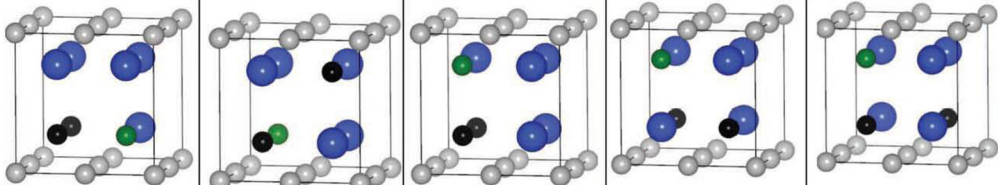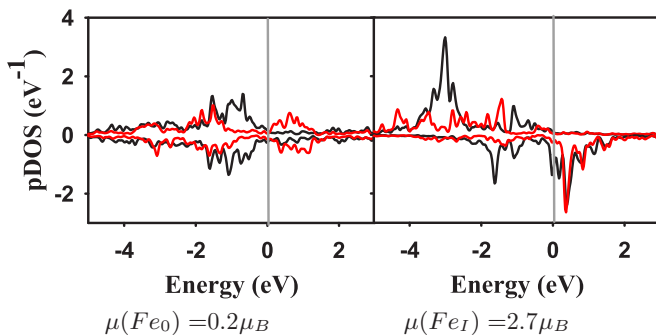
TABLE II. The ordered alloys with three substitutional Fe atoms at the Si sites. Si atoms are shown by blue balls, host Fe_0 by grey, substitutional Fe_I and Fe_{II} atoms are shown by black and green balls, correspondingly.

$\mu(Fe_0)$, μ_B $\mu(Fe_I)$, μ_B $\mu(Fe_{II})$, μ_B	0.5 2.6 −2.4	0.3 2.0 −2.0	0.8 2.6 2.3	1.0 2.4 2.2	1.0 2.6 2.3
Lattice parameter, Å	$a=b=5.23$ $c=5.37$	$a=5.12$ $b=5.23$ $c=5.37$	$a=5.23$ $b=5.37$ $c=5.33$	$a=b=5.18$ $c=5.50$	$a=b=5.27$ $c=5.44$

constant all on-site parameters (see Sec. II): Hubbard $U = 1$, i.e., all other parameters are given in units of U; $J = 0.4$, $\varepsilon_{Si} = 6$, and $\varepsilon_{Fe} = 0$. The calculations for different sets of parameters show that it is not the absolute values of the on-site energies that are important but rather their relative positions. So, we put $\varepsilon_{Fe} = 0$ and fit the energies ε_{Si} from the condition of the matching of the number of electrons on the Fe and Si atoms in the DFT and model calculations for all considered here compounds. The constant of the exchange interaction between nearest Fe atoms $J' = 0.05$ was taken the same for all compounds due to the small distance between the nearest neighbors Fe-Fe . So , even after these simplifications, we have to work in a five-dimensional space, since the model still has five hopping parameters: t_1 (Fe-Fe) and t_2 (Fe-Si) between the nearest neighbors (NN), t_3 (Fe-Fe), t_4 (Fe-Si) between next-nearest neighbors (NNN), and t_5 for Si-Si hoppings. The relation $t_\pi = \frac{1}{3}t_\sigma$ for NN and $t_\pi = \frac{1}{2}t_\sigma$ for NNN was kept in all model calculations; for this reason, hereafter, we will use $t_\sigma \equiv t$. The values for these hopping parameters are found from the requirement that after achieving self-consistency in both the model and the *ab initio* calculations (GGA), the d-DOS and magnetic moments on Fe atoms have to be as close to each other as possible. The best fit of the model magnetic moments and DOS to the *ab initio* ones can be achieved only when the hopping integrals are positive for the NN and negative for NNN. Along all model calculations we used equilibrium lattice parameters, obtained from the *ab initio* calculation (see Table I). We also take into account that the values of hopping

integrals should correlate with the distance between neighbors in all ordered alloys and in α-FeSi$_2$. The values of hopping parameters that provide the best fit are shown in the Table III.

1. α-FeSi$_2$

We begin with the stoichiometric α-FeSi$_2$ [Fig. 1(a)]. It has the tetragonal lattice with the space group $P4/mm$. Each of Fe atom in the α-FeSi$_2$ has only Si atoms in the nearest local environment and only Fe atoms as the second neighbors. These three hopping integrals, between NN Fe-Si (t_2), between NNN Fe-Fe (t_3), and between Si-Si (t_5) were used as fitting parameters as was discussed in Sec. II.

As criteria of fitting we used the best possible proximity of the model (i) population numbers, (ii) the magnetic moments on Fe atoms, and (iii) the partial density of d-electron states on Fe atoms to their GGA counterparts. Besides, it was required that the values of hopping integrals in all ordered alloys and in α-FeSi$_2$ (see above) correspond to the distance between neighbors, i.e., if the distance between first or second neighbors in any compound is larger then the value of the corresponding hopping integral should be smaller and vice versa.

The values of t_2, t_3, and t_5 parameters, which provide the best fitting in stoichiometric α-FeSi$_2$and its Fe-rich alloys, are shown in Table III. At these sets of the model parameters, the d-orbital population numbers $n_\uparrow^d$ and $n_\downarrow^d$ on Fe atoms in average deviate from the DFT ones by 6%–10% [see Table IV for (α-FeSi$_2$); not given here for the Fe-rich alloys]. This choice

TABLE III. The distances d (Å) between nearest neighbors (NN) and next-nearest neighbors (NNN) and the values of hopping integrals t, which provide the best fit of the model charge densities to the GGA-DFT ones.

	α-FeSi$_2$		B		C		D	
	d	t	d	t	d	t	d	t
Fe-Si (NN)	2.36	1.0	2.38	0.95	2.37	1.0	2.39	0.95
Fe-Fe (NN)	–	–	2.40	0.9	2.44	0.85	2.43	0.85
Fe-Si (NNN)	–	–	2.62	−0.55	2.24	−0.8	2.56	−0.45
Fe-Fe (NNN)	2.70	−0.65	2.60	−0.70	2.53	−0.75	2.56	−0.72
							2.78	−0.60
Si-Si (NN)	2.34	2.0	2.39	2.0	2.53	1.5	2.41	2.0
Si-Si (NNN)	2.80	1.0	2.61	1.5	–	–	2.78	1.0

TABLE IV. The comparison of orbital population numbers ($n_\uparrow^d$, $n_\downarrow^d$), magnetic moments (μ), and the number of electrons (N_{el}) for α-FeSi$_2$ in the model with GGA-DFT ones. The *ab initio* (blue lines) and the model (black lines) pDOS of Fe d electrons (left: t_{2g} electrons, right: e_g electrons) in α-FeSi$_2$ are compared in the figure under the table.

	VASP			Model		
	$n_\uparrow^d$	$n_\downarrow^d$		$n_\uparrow^d$	$n_\downarrow^d$	
d_{xy}	0.77	0.76	$\mu = 0.1\mu_B$	0.67	0.66	$\mu = 0.2\mu$
d_{xz}	0.72	0.71	$N_{el} = 6.6$	0.70	0.68	$N_{el} = 6.6$
d_{yz}	0.72	0.71		0.79	0.68	
$d_{x^2-y^2}$	0.58	0.55		0.63	0.61	
d_{z^2}	0.67	0.63		0.70	0.60	
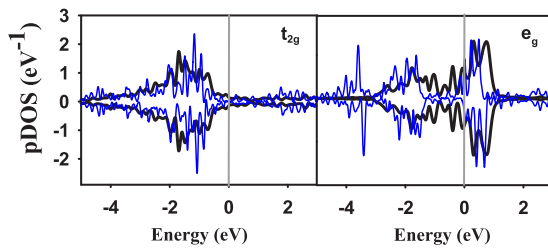
provides fine agreement between the DFT and model magnetic moments (μ) and the number of electrons (N_{el}) [Table IV (α-FeSi$_2$), Sec. B2 (Fe-rich alloys)]. The corresponding partial model and DFT DOSs for Fe d electrons in α-FeSi$_2$ are compared in the bottom of the Table IV. We have to emphasize again that in the model many matrix elements are neglected compared to the DFT approach. Therefore we should not expect a detailed matching of the model DOS to the DFT one. Qualitatively, nevertheless, the model DOS acquires the main features, which appear in the *ab initio* pDOS at this choice of parameters both for α-FeSi$_2$ (Table IV) and for the Fe-rich alloys (for example, see Fig. 6).

In order to understand the effect of NN and NNN neighbors in the local environment on the magnetic moment (MM) formation, we calculated the dependence of the MMs on the hopping integrals t_2 (NN Fe-Si) and t_3 (NNN Fe-Fe). The map of the magnetic moment dependencies on the hopping integrals t_2 and t_3 is shown in the top panel of Fig. 3. As seen, the crucial role in the MM formation is played by hoppings between NNN Fe-Fe (t_3). Indeed, with $|t_3| > 0.6$, the experimentally existing nonmagnetic state is stable, a decrease of $|t_3|$ leads to the transition into a ferromagnetic state. Furthermore, the boundaries between regions with magnetic states and nonmagnetic ones are very sharp (Fig. 3, top): the MM decreases till zero very fast as a function of hopping t_3 between iron atoms. The hopping between NN Fe-Si (t_2) has effect only on the magnitude of the MM in the ferromagnetic region. The mechanism of ferromagnetism destruction with hopping t_3 is clearly seen from the bottom panel of Fig. 3. Switching off the hopping between NNN Fe-Fe ($t_3 = 0$) makes the d bands atomlike with a slight smearing. An increase of the t_3 hopping leads to a delocalization of these atomlike d bands and destruction of the magnetism. Hence an increase of the distance between NNN (or, a decrease the hopping integral t_3) would result in a transition from a nonmagnetic
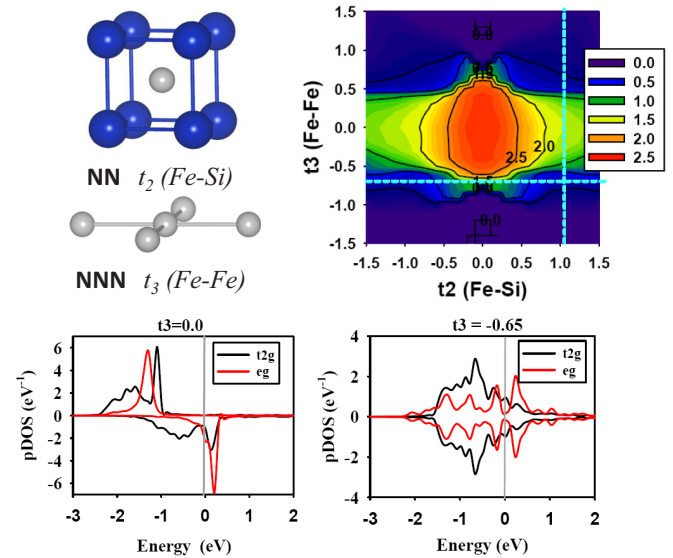

FIG. 3. (Top) Nearest and next-nearest neighbors of Fe$_0$ with corresponding hopping integrals (Fe and Si atoms are shown by grey and blue balls, correspondingly) and the t_2-t_3 map of magnetic moments; the blue lines show the values of hopping integrals t_2 and t_3 from Table IV. (Bottom) Model pDOS for hopping integral $t_3 = 0.0$ (left) and $t_3 = -0.65$ (right). Hopping integral $t_2 = 1.0$.

phase to a magnetic one. This conclusion from the analysis of the model is confirmed by the *ab initio* calculation: the increase of the lattice parameters a and b of α-FeSi$_2$ (or the distance NNN Fe-Fe) by 7% ($a = b = 2.9$ Å and $c = 5.13$ Å) causes formation of MMs $\mu = 0.6\mu_B$ on the Fe atoms. Thus it is rather the hopping integral between the NNN Fe-Fe atoms, not the NN Fe-Si hopping, that determines the existence of a magnetic or a nonmagnetic state in α-FeSi$_2$, because the NN of Fe atom consist of Si atoms in both cases.

2. Fe-rich alloys

To emphasize the importance of the NNN in the MM formation on iron atoms, we consider the alloys C and D from Table I. These alloys reveal essentially different magnetic behavior at the same concentration but different spatial arrangements of the substitutional Fe atoms.

As it follows from *ab initio* calculations, the ordered alloy D reveals ferromagnetism, whereas alloy C remains nonmagnetic (Table I). These ordered alloys have two nonequivalent Fe atoms: Fe$_0$ is the host iron atom in the iron sublattice of α-FeSi$_2$ and Fe$_I$ is the substitutional Fe atoms in the Si sublattice. Different spatial arrangement of the substitutional Fe atoms results in the different environment of the host and substitutional Fe atoms in alloys D and C. These environments are shown in Fig. 4 (top). There is an important difference in the NNN environment of Fe$_0$ and Fe$_1$ in C and D alloys. In the C alloy both Fe$_0$ and Fe$_I$ atoms have four Fe atoms along crystallographic axes a and b as NNN at the same distances $R = 2.53$ Å (Table III). The host Fe$_0$ in the alloy D also has four NNN Fe atoms, but at different distances: two Fe neighbors along axis a with the distance $R = 2.56$ Å and two ones along axis b with $R = 2.78$ Å. These unequal distances arise due to the different symmetry of crystal lattices:
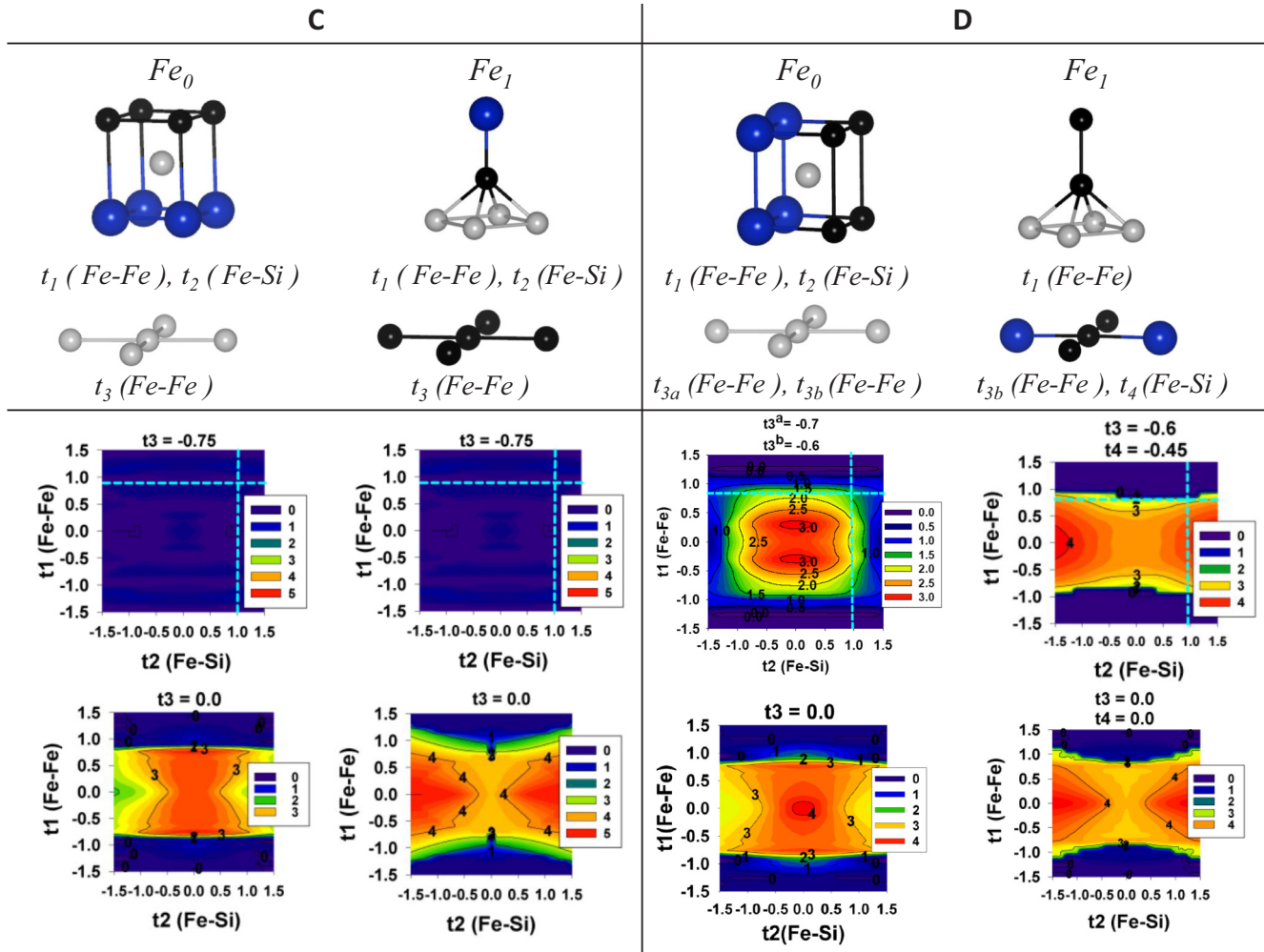
FIG. 4. Alloys C and D. (Top) NN and NNN environment of iron atoms. Si atoms are shown by blue balls, grey and black balls stand for Fe_0 and substitutional Fe_I atoms, correspondingly. (Middle) Dependence of the MMs on hopping integrals t_1 and t_2 (hopping integrals t_3 and t_4 are switch on). (Bottom) Dependence of MMs on hopping integrals t_1 and t_2 (hopping integrals t_3 and t_4 are switch off). Blue lines show the values of hopping integrals $t_1 = 0.9$ and $t_2 = 1.0$ for alloy C and $t_1 = 0.85$ and $t_2 = 0.95$ for alloy D (Table III); these values provide the best fitting to the *ab initio* charge density.

the C lattice is tetragonal with the space group $P4mm$, while the D one is orthorhombic with space group $Pmmm$. Thus the distortions of the underlying tetragonal lattice of α-FeSi$_2$ arising in these alloys are different. Notice that the distances between the NN Fe-Si and the NN Fe-Fe in both alloys are the same. Besides, the atom Fe_I has only two NNN Fe atoms at the distance $R = 2.78$ Å in the alloy D. This distance is larger than the corresponding one in alloy C. Therefore we are forced to introduce in alloy D two hopping integrals for the short t_3^a and long t_3^b distances between NNN Fe-Fe, while only one hopping integral t_3 is required for the description of alloy C. The values of hopping integrals providing the best found fitting to the *ab initio* calculation according to Eq. (2) are given in Table III. The Hartree-Fock self-consistent MMs generated by the model at these values of hopping parameters are $\mu^{mod}(Fe_0) = \mu^{mod}(Fe_1) = 0$ in alloy C and $\mu^{mod}(Fe_0) = 1.4\mu_B$, $\mu^{mod}(Fe_1) = 2.5\mu_B$ in alloy D.

Let us compare the dependencies of the Fe magnetic moments on the NN hopping integral t_1 and t_2 at fixed values of NNN hopping integral t_3 and t_4, shown at the middle panel

of Fig. 4. The range of the magnetic moments existence on both Fe_0 and Fe_I atoms in alloy D is restricted by the values of $|t_1| < 1$. The magnetic state with moments close to *ab initio* values $[\mu(Fe_0) = 1.5\mu_B$ and $\mu(Fe_I) = 2.5\mu_B]$ is on the narrow boundary between ferro- and paramagnetic phases. In alloy C, the nonmagnetic state is stable in all ranges of the hoppings between NN t_1 and t_2. Namely, the circumstance that the magnetic moments are close to the instability line make them very sensitive to changes of the NNN hoppings. Indeed, which of the solutions, magnetic or nonmagnetic, will arise, is controlled by the value of hopping integral t_3: t_3^C(Fe-Fe) $=$ -0.75 leads to the formation of the paramagnetic state in alloy C, whereas a decrease of t_3 in alloy D, t_3^D(Fe-Fe) $= -0.60$, gives birth to a ferromagnetic state in alloy D. The increase of $|t_3^C$(Fe-Fe)$|$ compared to $|t_3^D$(Fe-Fe)$|$ occurs due to the shorter distance between Fe atoms in the NNN environment in alloy C (Table III). Moreover, a decrease of $|t_3|$ results in the appearance of magnetic moments on both Fe atoms in alloy C; at $t_3^C = 0.0$, the map of magnetic moments in alloy C becomes similar to the one for alloy D (Fig. 4, bottom). At first glance,
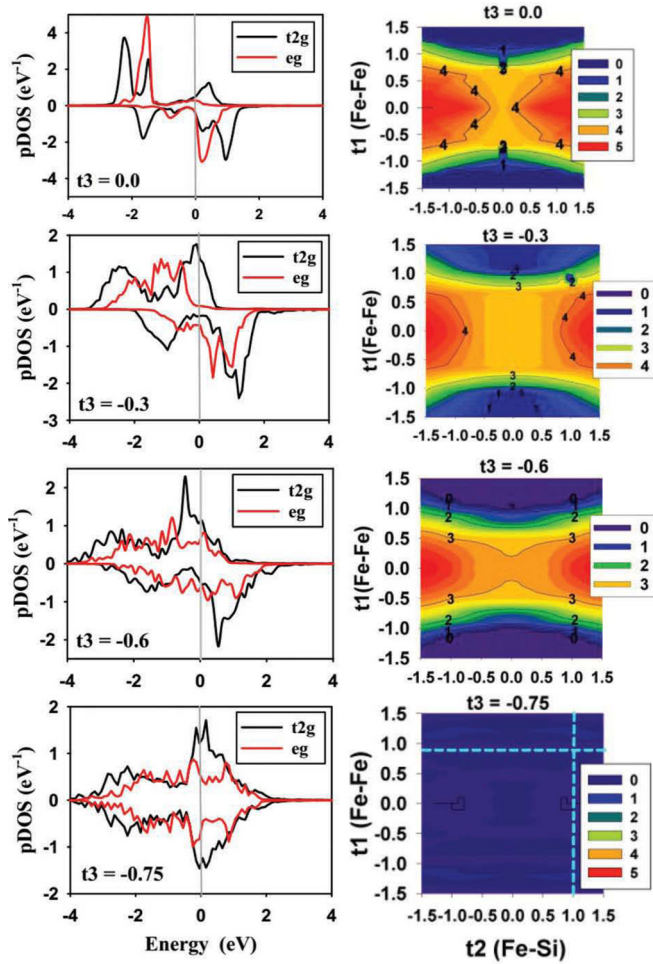
FIG. 5. Alloy C: model pDOS (left panel) and the map of the magnetic moments (right panel) for the different values of hopping integral t_3(Fe-Fe). The blue lines at the last map show the values of hopping integrals $t_1 = 0.9$ and $t_2 = 1.0$ (Table III), which provide the best fitting to the *ab initio* charge density.

FIG. 6. The comparison of the *ab initio* (blue lines) and the model (black lines) pDOS of Fe_I d electrons (left) and Fe_{II} d electrons (right) in alloy B. (Top) t_{2g} electrons and (bottom) e_g electrons.

one could expect that the formation of the Fe-Si bond should destroy the moment on the Fe atom. However, the magnetic moments on Fe atoms happen to be much less sensitive to the hopping parameter t_2 between NN Fe and Si atoms. Indeed, all the t_1-t_2 maps for Fe moments, calculated within this model, are elongated along the axis t_2.

The physics of the destruction of the magnetic moments on Fe atoms can be interpreted from the point of view of the d-band formation. Figure 5 illustrates this for alloy C via the evolution of the Fe_I d-electron pDOS and the corresponding magnetic-moment maps with the increase of only the hopping integral t_3 while all other hopping integrals are kept fixed. As seen, at the first steps of increase of t_3, a gradual smearing of initially (at $t_3 = 0$) atomlike levels and a slight change of the map of magnetic moments occurs. Then, similar to the case of α-FeSi$_2$, at $t_3 = -0.75$, an abrupt destruction of the magnetic moments arises and the difference between the minority and majority spin states in pDOS disappears.

Let us now discuss the origin of the unusual ferrimagnetic state in the type of alloy B (Table I) that contains three substitutional Fe atoms on the Si sites. The ordered alloy B
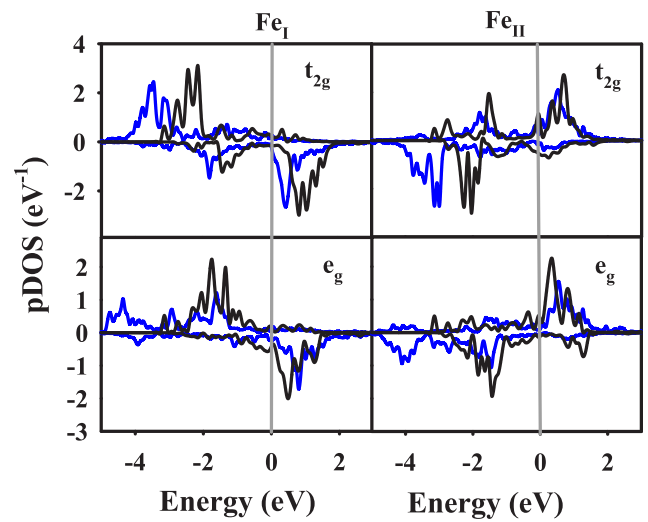
has the tetragonal lattice with space group $P4mm$. There are three nonequivalent Fe atoms in the unit cell: Fe_0 is the host iron sublattice of α-FeSi$_2$, Fe_I, and Fe_{II} are the nonequivalent substitutional Fe atoms in the Si sublattice. In accordance with *ab initio* calculations, the absolute values of magnetic moments on Fe_I and Fe_{II} atoms are close to each other but have *opposite* directions: $\mu(Fe_I) = 2.3\mu_B$ and $\mu(Fe_{II}) = -1.9\mu_B$. The model MMs obtained for the values of hopping integrals from Table III are $\mu^{mod}(Fe_I) = 2.8\mu_B$, $\mu^{mod}(Fe_{II}) = -2.1\mu_B$, and $\mu^{mod}(Fe_0) = 0.7\mu_B$. The specific feature of Fe pDOS in the alloy B is that the Fe_{II} pDOS is mirror-symmetric to the pDOS of Fe_I atoms. This feature arises in both first-principles and model calculations. The comparison of pDOSs for substitutional Fe atoms is shown in Fig. 6. As in previous cases, we built the t_1-t_2 maps of MMs for three nonequivalent Fe atoms (Fig. 7). The bright illustration of the importance of NNN interactions is that in spite of the fact that the NN local environment of substitutional Fe atoms is the same (Fig. 7, first column), they have completely different maps of magnetic moments. There is a wide range (at $|t_1| \gtrsim 0.5$) of negative MMs in the map for Fe_{II} atom (Fig. 7, bottom panel, middle column) with a sharp boundary between positive and negative values of MMs, whereas in the same region of the Fe_I t_1-t_2 map, the MM remains positive. These distinctions occur due to the different number of Fe atoms in the NNN environment. Indeed, switching off the hoppings between NNN neighbors (t_3 and t_4) changes the behavior of magnetic moments on Fe_{II} atom: the region with the negative moment disappears and the maps for Fe_I and Fe_{II} atoms became almost identical (cf. middle and bottom panels in Fig. 7, last column). This numeric experiment explicitly shows that the role played by the NNN local environment is critically essential for the emergence of the Fe atoms with the opposite MMs and, correspondingly, for the development of the ferrimagnetic state.

Thus our analysis of the Hartree-Fock solutions of the multiorbital models of iron silicides and the supporting first-principles calculations allow us to conclude that the decisive
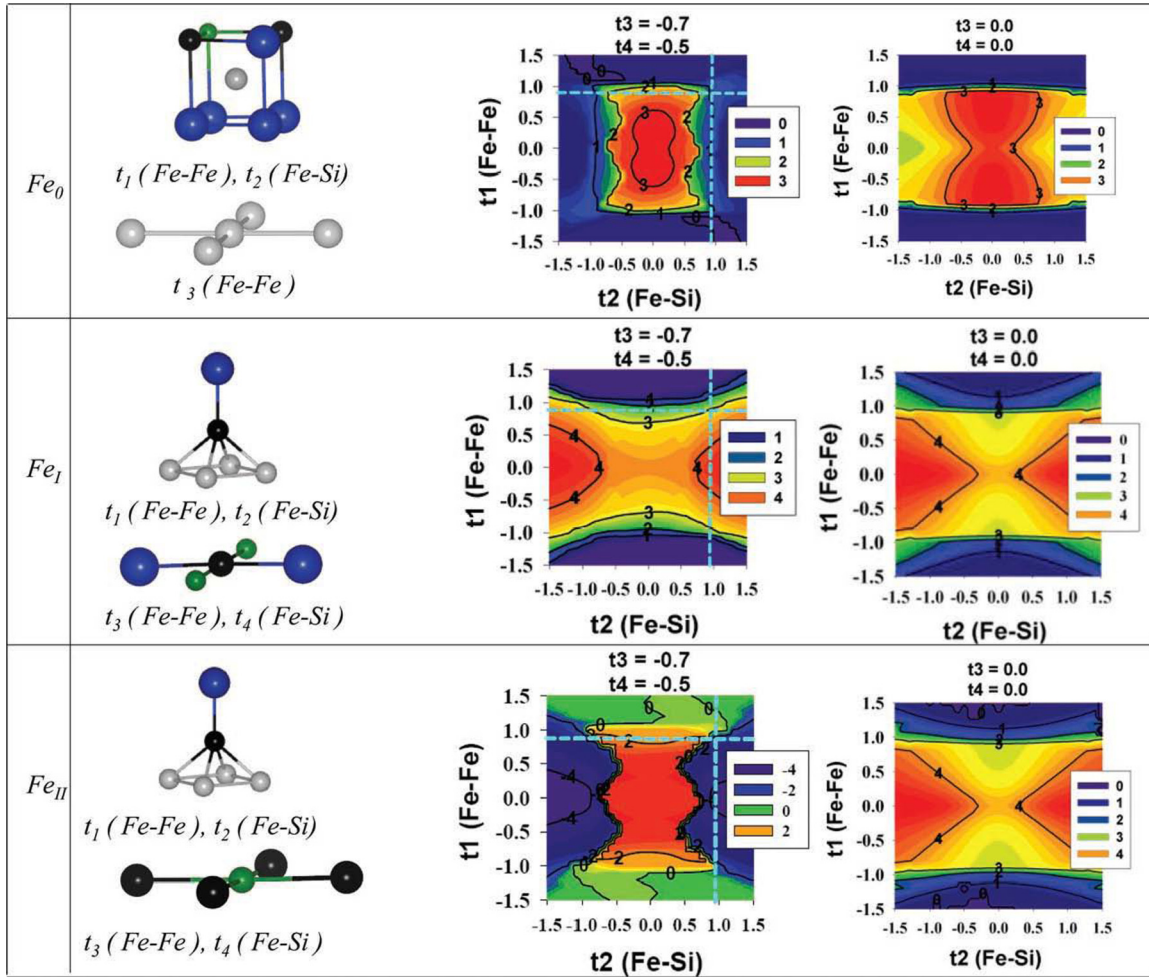
FIG. 7. Alloy B. (Top, left) NN and NNN environment of Fe_0 atoms; color encodings: Si are blue, Fe_0 are grey, substitutional Fe_I and Fe_{II} are black and green balls, correspondingly. (Top, center) The dependence of Fe_0 MMs on hopping integrals t_1 and t_2 (hopping integrals t_3 and t_4 are switch on). (Top, right) The dependence of MM on the Fe_0 atom on the hopping integrals t_1 and t_2 (hopping integrals t_3 and t_4 are switch off). (Middle and bottom) Same for Fe_I and Fe_{II} atoms, correspondingly. Blue lines on the maps show the values of hopping integrals $t_1 = 0.9$ and $t_2 = 0.95$ (Table III), which provide the best fitting to the *ab initio* charge density.

role in the destruction/formation of the iron magnetic moments is played by the NNN local environment or, more specifically, by the number of neighbors Fe-Fe and the by the spacing between them. The results of our calculations show that the previous statement [26–28], that the destruction of magnetic moments in the iron silicides is caused by the increase of Si atoms in the NN environment is inaccurate. The obtained in our calculations strong influence of NNN Fe-Fe couples is caused by the peculiarity of the α-$FeSi_2$ crystal structure, where the the iron atoms form planes. Since NNN Fe-Fe are arranged along crystallographic axes, strong σ bonds between Fe atoms are formed. So in alloy C and α-$FeSi_2$, which contains iron (001) planes with a shorter distance between Fe-Fe than in alloy D, these d bonds result in the delocalization of the electrons and a decrease of the MMs up until their destruction (Fig. 5). At the same time in alloys C and D, Fe atoms have the same number of Si atoms in the NN environment and this does not prohibit them to have different MMs. It is very instructive to have a look from this point of view at the MM formation in

alloy A where the substitutional Fe atoms have maximal MMs compared to the ones in all other alloys considered here. The NNN environment of the substitutional Fe_I atom in alloy A (Table I, first column) consists of only Si atoms; the hoppings between Fe-Fe, which are responsible for the destruction of moment are absent. This facts lead to the formation of a large value of MM on this iron atom.

In order to demonstrate the decisive role of the d-d-hopping integral t_3 between NNN Fe-Fe on the formation of the MM on Fe atoms, we calculate the dependence of Fe MM on this hopping for α-$FeSi_2$ and the alloys C and B. This dependence is shown in Fig. 8. As seen, the increase of t_3 in alloy C and in α-$FeSi_2$ causes a destruction of the Fe MMs, whereas in alloy B the abrupt flip of the Fe_{II} magnetic moment occurs with an increase of t_3. The model results are confirmed by the *ab initio* calculations. Obviously, the hopping integral t_3 changes its value with an increase of the spacing between NNN Fe-Fe. Since the integral of the hopping matrix element contains an overlap of the wave functions, we assume that it depends on
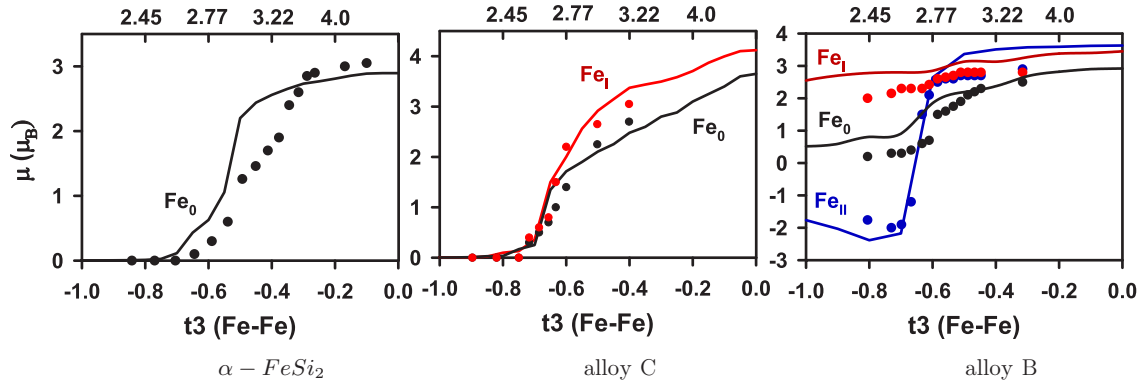
FIG. 8. The dependence of MMs on the host Fe_0 and the substitutional Fe_I and Fe_{II} atoms on hopping t_3 in α-$FeSi_2$, alloys C and B (from left to right). The solid lines are the dependencies, obtained in model calculations, the dots show the MMs from *ab initio* calculations at a distance R between NNN Fe-Fe, according to (6). The scale for the distances (in angstroms) is given on the top of the figures.

the distance R between the ions exponentially,

$$t_3(R) = t_3^{\max} \exp(\gamma \Delta R), \qquad (6)$$

where $t_3^{\max} = t_3(R_{\min})$ and $\Delta R = R - R_{\min}(\text{Å})$. Taking the values $t_3^{\max} = -0.75$ and $R_{\min} = 2.53$ from Table III, we have found the parameter $\gamma = -0.8926\,\text{Å}^{-1}$. Using Eq. (6), we obtained the distances R between NNN Fe-Fe corresponding to the model parameters t_3. Then the values of the MMs for the lattice parameters corresponding to these distances have been calculated within the GGA-to-DFT approach. These values are shown in Fig. 8 by dots. Remarkably, although only t_3 hopping was changed with distance R in the model calculations (the values of the other hopping parameters were kept fixed according to Table III), we obtained a good agreement between the model and the *ab initio* magnetic moments. This again proves the significance of the NNN Fe-Fe couplings for the MM formation.

.

C. *Ab initio* calculation of the Si-rich alloys

Our model calculations lead to the conclusion that the Fe local MM formation is controlled either by a decrease of the number of Fe-Fe couples in Fe layers or by an increase of the distance between Fe atoms in pairs. Moreover, we can state that the increase of the cell' s magnetic moment with increase of x in Fe-rich alloys $Fe_{1+x}Si_{2-x}$ is associated namely with the appearance of high-spin Fe species in the Si layers, which are surrounded mainly by the Si atoms. However, these conditions can be fulfilled also by an increase of the Si concentration. To make sure that this unexpected conclusion derived from the model is correct, we carried out the *ab initio* GGA calculation of Fe magnetic moments for the Si-rich ordered alloys $Fe_{1-x}Si_{2+x}$. The alloy structures must satisfy the conditions listed above. By adding Si atoms into the iron planes, we can decrease the number of the Fe-Fe couples. Besides, the substitutional Si atoms increase the spacing between the Fe atoms.

Figure 9 displays three different variants of substitution of Fe atoms in the Fe planes by the Si atoms. All calculations were carried out for the supercells $2a \times 2b \times 2c$ of α-$FeSi_2$, containing six iron atoms and two additional Si atoms. After

full optimization of the supercells, all considered alloys become magnetic, but the magnitude of the magnetic moment μ per supercell depends on the particular arrangement of substitutional Si atoms: $\mu = 3.2\mu_B$ [Fig. 9(a)], $\mu = 3.1\mu_B$ [Fig. 9(b)], and $\mu = 1.7\mu_B$ [Fig. 9(c)]. The emergence of local MM on different Fe atoms in the first two alloys [Figs. 9(a) and 9(b)] corresponds to the expectations, derived from the model. Indeed, since the number of iron NNN surrounded an Fe_3 atom in the first alloy [Fig. 9(a)] is decreased by two, a local magnetic moment $\mu(Fe_3) = 0.8\mu_B$ on the Fe_3 atom arises. Similarly, local MM appears on the Fe_1 and the Fe_5 atoms in the second alloy [Fig. 9(b)] due to an increase of the distance between NNN Fe-Fe till $\simeq 2.8$ Å. The third alloy [Fig. 9(c)], however, presents an example where, it seems, the model is oversimplified: the GGA calculation produces zero moment on the Fe_5 atom without Fe atoms in NNN surrounding, while according to our model the biggest local magnetic moment have to arise on the Fe_5 in this case. We assume that the term responsible for it and which is missed in our model is the crystal electric field (CEF), created by the Si surrounding. The Fe_5 in the third alloy [Fig. 9(c)] sits in the most symmetrical local surrounding $P4/mmm$ by Si atoms, where the CEF splitting has to be stronger than in the first two cases [Figs. 9(a) and 9(b)].

One can see from Fig. 9 that the lattice parameters in all Si-rich alloys are larger than the ones in the stoichiometric α-$FeSi_2$. However, the appearance of ferromagnetism in the compounds is not related to the lattice strain. To prove it, we performed DFT calculations for three stoichiometric α-$FeSi_2$ structures with lattice parameters from Fig. 9. Only lattice strain is insufficient for the emergence of the Fe atoms magnetic moments. So, in the structure with the lattice parameters from Fig. 9(c), the magnetic moment does not appear, for the other two sets of the lattice parameters the Fe magnetic moments are about $\mu = 0.2\mu_B$. Therefore we come to the counterintuitive conclusion: it is the increase of the Si atoms concentration that is responsible for the emergence of magnetism, not the strains.

The statement that the magnetic moments in Fe-Si alloys can arise due to an increase of the Si concentration allows us to suggest an alternative explanation of the ferromagnetism in the α-$FeSi_2$ (111) film on the Si(001) substrate, successfully

$a=5.72$ Å $b=5.42$Å $c=10.35$Å

$\mu(Fe_1)=\mu(Fe_2)=0.42\,\mu_B$
$\mu(Fe_3)=0.78\,\mu_B$

$a=b=5.54$Å $c=10.38$Å

$\mu(Fe_1)=\mu(Fe_5)=0.80\mu_B$
$\mu(Fe_2)=\mu(Fe_6)=0.31\mu_B$
$\mu(Fe_3)=\mu(Fe_4)=0.45\mu_B$

$a=b=5.61$Å $c=10.24$Å

$\mu(Fe_1)=\mu(Fe_4)=0.50\mu_B$
$\mu(Fe_2)=\mu(Fe_3)=0.35\mu_B$
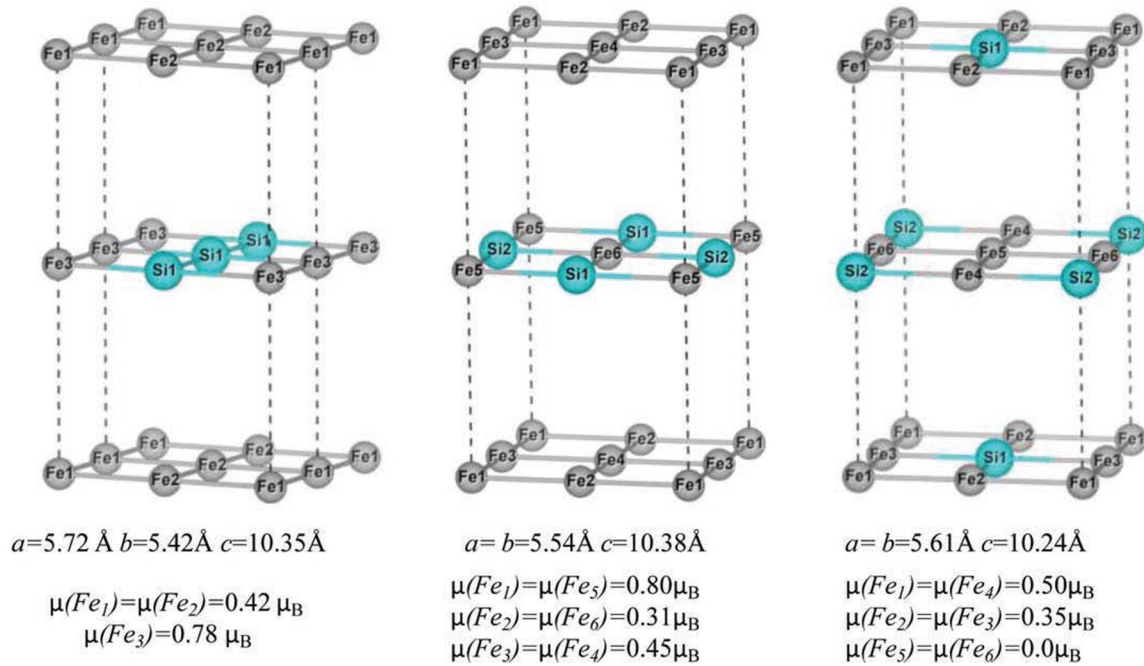$\mu(Fe_5)=\mu(Fe_6)=0.0\mu_B$

FIG. 9. Different environments for Fe ions lead to the formation of local MMs when part of the Fe ions are replaced by Si ions (the host Si atoms are not shown). The optimized lattice parameters and the calculated MMs of the Fe atoms are given under the structures.

stabilized by the authors of Ref. [24]. The authors of Ref. [24] explain the ferromagnetism of the α-FeSi$_2$ film by the small concentration (about 3%) of the additional substitutional Fe atoms. The calculation in Ref. [24] were performed in the framework of CPA, which is not able to take into account the local-environment effects. We assume that the observed moment arises not due to an increase of the Fe concentration as stated in the work [24], but due to an increase of Si concentration that arises due to a diffusion of the Si atoms from the Si substrate. For example, the lattice parameters in the considered here Si-rich alloys are such that the (111) elementary-cell sizes of the α-FeSi$_2$ are very close to the Si(001) $-$ (3×2)(11.5×7.68 Å): (11.83×7.89 Å), (11.76×7.83 Å), and (11.67×7.93 Å) for the first [Fig. 9(a)], second [Fig. 9(b)], and third [Fig. 9(c)] alloys, correspondingly. This corresponds to the mismatch about (-1.5%)–(-2.5%). Such a low mismatch presents an opportunity to stabilize the epitaxial films of the α-FeSi$_2$ structure with similar arrangements of Si atoms. The magnetic moment $\mu \approx 0.2$–$0.4\,\mu_B$/f.u. arises for all types of the substitutions shown in Fig. 9, which is consistent with the observed in Ref. [24] values.

IV. CONCLUSIONS

The fact that a large, if not the decisive, role in the mechanism of the magnetic structure formation in different compounds is played by the local environment of the magnetic species is well known from the physics of surfaces and interfaces. The effects of local environment are especially important in alloys, in which a slight difference in the local environment can result in significantly different magnetic structures. The substitutionally disordered systems such as metallic alloys play an increasingly important role in techno-

logical applications and, hence, a lot of efforts are invested into a theoretical understanding of their properties. Although CPA is nowadays the most successful *ab initio* theoryfor the calculations of disordered alloys, its standard formulation neglects the effects of NNN environment. Along with the development of *ab initio* methods (as nonlocal CPA [40]), an understanding of a specific property of a specific compound can be reached in the framework of suitable models with parameters obtained from *ab initio* calculations for a the material of interest. A combination of the *ab initio* and the multiorbital-model calculations for the iron silicides was used in our work. We consider the model by the perturbation theory from the weak-coupling side. This places the model to the class of the itinerant-electron models. Our model, compared to the Stoner's one, is strongly improved: here the magnetism is formed not due to just Stoner's parameter, but due to all main intra-atomic interactions. It is shown that certain type of hopping terms control the formation of magnetism. One of the advantages of the suggested approach is that, on the one hand, it is a model approach, which allows to apply the standard diagram perturbation theory and, therefore, to consider excitations, thermodynamics, etc. On the other hand, it is a first-principles approach, since it does not contain any parameters, which should be fitted from experiment. The reason why we chose the mean-field approximation for the first-step model consideration (which for the itinerant electrons is the Hartree-Fock approximation) is that any next approximation in the model contains spin waves, damping of the excitations, and their spectral weights, the characteristics of which can not be extracted from the Kohn-Sham scheme. Since the model does not contain local moments, the words "formation of the magnetic moment" (local characteristics) and "emergence of the magnetic phase" (long-rage order) are not distinguishable within the used approximation. Clearly,

a deeper understanding of the magnetism nature in these compounds requires calculation of the temperature-dependent magnetic susceptibilities. In turn, the latter requires the knowledge of the spin-waves spectra and their decay, the interaction of collective excitations with conduction electrons, and the degree of the on-site moment fluctuations. However, the following are unavoidable necessary first steps: (a) formulation of the model, (b) calculation of its properties within the Hartree-Fock approximation, and (c) finding the parameters for real materials by fitting the model density of electrons to the *ab initio* one. These steps and the analysis of the results, which are controlled by first-principles calculations, are presented in our work and are the essence of the suggested method of hybrid *ab initio and model calculation method* (HAI MCM). The feature (c) distinguishes our model approach from other ones. The model consideration presents an opportunity to elucidate the role played by the effects of NN and NNN local environment of the Fe atoms on the formation of magnetic moments. The feature that distinguishes our model approach from other ones is that the parameters of the model are determined by fitting its self-consistent charge density to the one obtained by *ab initio* calculations. This allows to study the effects of NN and NNN local environment of the Fe atoms on the formation of magnetic moments.

The presented study of the effect of silicon-atoms' substitution by the iron atoms and vice versa on the magnetic properties in the iron silicide α-FeSi$_2$ within the suggested multiorbital model has shown that while the stoichiometric material α-FeSi$_2$ is nonmagnetic, the appearance of substitutional iron atoms in the α-FeSi$_2$ may result in different magnetic structures, either ferromagnatic or ferrimagnetic. Which particular structure emerges is determined by the number and the *spatial arrangement* of the substitutional iron atoms. The latter statement is strongly supported by the fact that different magnetic structures can appear at *the same* concentration of substitutional Fe atoms. Besides, as follows from the Hartree-Fock model calculations, the formation of magmetic moments is essentially determined not by the NN Si atoms but by the NNN environment, particularly, by the Fe atoms along the crystallographic axes: the MMs on iron atoms are very sensitive to the values of NNN Fe-Fe hopping parameters t_3. We demonstrated it by a comparison of the maps of moments' dependence on the hopping parameters with and without contributions from NNN. It is important that the nonmagnetic states in the stoichiometric α-FeSi$_2$ arise at NNN $t_3 \neq 0$ only. The model with NN hoppings only, even if all NN to Fe atoms are Si atoms, does not have the solutions with zero moments on Fe. This allows us to suggest that the magnetism in the nonmagnetic α-FeSi$_2$ can be induced by a negative pressure.

The various magnetic structures (ferro-, ferri-, or nonmagnetic) in Fe-rich alloys are also controlled by the NNN Fe-Fe hopping parameters t_3. The different ways of Si atom substitution by Fe atoms result in the diverse local distortions of the underlying lattice and, in turn, to quite different hopping parameters t_3 and magnetic properties. It is most clearly demonstrated by the magnetic behavior of several alloys with the same concentration of substitutional atoms, e.g., alloys C and D considered in this work (Sec. II B). The comparison of the magnetic-moments maps shows that namely the NNN

Fe-Fe hopping parameters t_3 are responsible for a nonmagnetic state in alloy C and a ferromagnetic one in alloy D. Notice that despite of the different lattice distortions in C and D alloys, the spacing between NN (as well as number of NN Si atoms) is the same in both cases. Hence the local environment models, which do not take into account the NNN hoppings, cannot explain this distinction. Unlike the local environment models [26,27], we observe that the dependence of the Fe magnetic moment on the hopping t_2 between NN Fe and Si atoms is weak; all the t_1-t_2 maps for Fe moments, calculated within this model, are elongated along the axis t_2. One more characteristic feature of the maps as a function of NN Fe-Fe hopping integral t_1 is the presence of sharp boundaries in the region between magnetic and nonmagnetic states. This part of the phase diagram is most interesting for possible applications. Indeed, one can expect that the system being in the vicinity of of the magnetic-instability line has to be much more sensitive to different external perturbations, than in other parts of the phase diagram (some suggestions how to use it are discussed below). For the same reason, it is not surprising that the contribution of the NNN interactions becomes important. It has to be emphasized that our conclusion about the decisive role of NNN local environment in the magnetic moment formation presents an alternative explanation to the conclusions of earlier (much less detailed) models of local environment [26,27], where a decrease of the moment on Fe atoms was ascribed to the increase of number of Si in NN sphere. According to our calculations, the main role in the formation of local magnetic moments is played by the decrease of the number of Fe-Fe pairs along the crystallographic axes and/or increase of the distance between them. This conclusion is especially interesting since most of models do not take the NNN hoppings into account.

The unexpected and somewhat counterintuitive conclusion, following from the model calculations, is that not only an increase of the Fe but also of the metalloid concentration can lead to the emergence of the local magnetic moment on Fe atoms. Indeed, the number of the Fe-Fe pairs can be reduced by replacing of the Fe atoms in iron planes by Si atoms. Moreover, the distances between Fe atoms in these planes are increased due to the distortion of the underlying lattice. So, the conditions leading to the emergence of the magnetism are met. The *ab initio* calculation of the ordered Si-rich alloys confirms this conclusion. Hence we can explain the ferromagnetism in the α-FeSi$_2$ (111) film, obtained by the authors of Ref. [24], in a more realistic way. In our opinion, the observed in Ref. [24] moment results from the increase of Si concentration due to a diffusion of the Si atoms from the Si substrate, but not due to an increase of the Fe concentration.

The presented analysis allows us to suggest a way for the stimulation of the magnetic state formation in iron silicides. The key parameters responsible for the magnetism are the hoppings between Fe atoms t_1 and t_3, which are the most sensitive parameters to different types of pressure. The latter can be done either by fitting the lattice parameter of the substrate for an α-FeSi$_2$ film (chemical pressure), or by a substitution of Fe or Si atoms. As was pointed out in Ref. [25], the best orientation relationships that stabilize the epitaxial α-FeSi$_2$ are α-FeSi$_2$ (201) $\parallel$ Si(110), α-FeSi$_2$ (110) $\parallel$ Si(110), or α-FeSi$_2$ (111) $\parallel$ Si(001). Such planes contain additional Si atoms in Si-rich alloys from Fig. 9 and the sizes of the

corresponding unit cells are very close to the Si-substrate one. A small mismatch has been placed for all mutual orientations of the film and the substrate and presents an opportunity to stabilize the epitaxial films of the α-FeSi$_2$ structure. Moreover, the possibility of tuning the hopping parameter t_3 in iron silicides has large technological interest because it gives an opportunity to control the appearance of different magnetic configurations in the cause of fabrication of new alloys or nanostructures with the prospective magnetic properties. At last, the existence of the region with sharp transition from ferro- to paramagnetic or from ferro- to ferrimagnetic state strongly improves the prospects for practical applications of iron-silicide films (like, e.g., switching on and off the magnetic state by external fields) and, hopefully, will stimulate

technologists to find a way to make films near the instability line with desirable characteristics.

[1] A. I. Liechtenstein, M. I. Katsnelson, and V. A. Gubanov, J. Phys. F **14**, L125 (1984); Solid State Commun. **54**, 327 (1985); A. I. Liechtenstein, M. I. Katsnelson, V. P. Antropov, and V. A. Gubanov, J. Magn. Magn. Mater. **67**, 65 (1987); M. I. Katsnelson and A. I. Lichtenstein, Phys. Rev. B **61**, 8906 (2000).

[2] L. Hedin, Phys. Rev. **139**, A796 (1965).

[3] L. J. Sham and M. Schlüter, Phys. Rev. Lett. **51**, 1888 (1983).

[4] L. J. Sham, Phys. Rev. B **32**, 3876 (1985).

[5] I. Sandalov, U. Lundin, and O. Eriksson, Int. J. Quantum Chem. **102**, 1019 (2005).

[6] I. Khmelevska, S. Khmelevskyi, A. V. Ruban, and P. Mohn, J. Phys.: Condens. Matter **18**, 6677 (2006).

[7] N. I. Kulikov, D. Fristot, J. Hugel, and A. V. Postnikov, Phys. Rev. B **66**, 014206 (2002).

[8] J. C. Slater and G. F. Koster, Phys. Rev. **94**, 1498 (1954).

[9] E. E. Fullerton, J. E. Mattson, S. R. Lee, C. H. Sowers, Y. Y. Huang, G. Felcher, and S. D. Bader, J. Magn. Magn. Mater. **117**, L301 (1992).

[10] K. Inomata, K. Yusu, and Y. Saito, Phys. Rev. Lett. **74**, 1863 (1995).

[11] J. J. de Vries, J. Kohlhepp, F. J. A. den Broeder, R. Coehoorn, R. Jungblut, A. Reinders, and W. J. M. de Jonge, Phys. Rev. Lett. **78**, 3023 (1997).

[12] R. R. Gareev, D. E. Buergler, M. Buchmeier, R. Schreiber, and P. Grunberg, J. Magn. Magn. Mater. **240**, 237 (2002).

[13] S. Yoon and J. G. Booth, Phys. Lett. A **48**, 381 (1974).

[14] A. Ionescu, C. A. F. Vaz, T. Trypiniotis, C. M. Gurtler, H. Garcia-Miquel, J. A. C. Bland, M. E. Vickers, R. M. Dalgliesh, S. Langridge, Y. Bugoslavsky, Y. Miyoshi, L. F. Cohen, and K. R. A. Ziebeck, Phys. Rev. B **71**, 094401 (2005).

[15] K. Seo, S. Lee, Y. Jo, M.-H. Jung, J. Kim, D. G. Churchill, and B. Kim, J. Phys. Chem. C **113**, 6902 (2009); S. A. Lyaschenko, Z. I. Popov, S. N. Varnakov, L. A. Kuzubov, S. G. Ovchinnikov, T. S. Shamirzaev, A. V. Latyshev, and A. A. Saranin, JETP **120**, 886 (2015).

[16] C. Kloc, E. Arushanov, M. Wendl, H. Hohl, U. Malang, and E. Bucher, J. Alloys Compd. **219**, 93 (1995).

[17] N. Jedrecy, A. Waldhauer, M. Sauvage-Simkin, R. Pinchaux, and Y. Zheng, Phys. Rev. B **49**, 4725 (1994).

[18] J. K. Tripathi, M. Garbrecht, W. D. Kaplan, G. Markovich, and I. Goldfarb, Nanotechnology **23**, 495603 (2012).

[19] Y. Dusausoy, J. Protas, R. Wandji, and B. Roques, Acta Crystallogr. B **27**, 1209 (1971).

[20] M. Seibt, R. Khalil, V. Kveder, and W. Schröter, Appl. Phys. A **96**, 235 (2009).

[21] S. Pan, C. Ye, X. Teng, H. Fan, and G. Li, Phys. Status Solidi A **204**, 3316 (2007).

[22] X. Lin, M. Behar, J. Desimoni, H. Bernas, J. Washburn, and Z. Liliental-Weber, Appl. Phys. Lett. **63**, 105 (1993).

[23] C. Detavernier, C. Lavoie, J. Jordan-Sweet, and A. S. Ozcan, Phys. Rev. B **69**, 174106 (2004).

[24] G. Cao *et al.*, Phys. Rev. Lett. **114**, 147202 (2015).

[25] J. K. Tripathi, G. Markovich, and I. Goldfarb, App. Phys. Lett. **102**, 251604 (2013).

[26] W. A. Hines, A. H. Menotti, J. I. Budnick, T. J. Burch, T. Litrenta, V. Niculescu, and K. Ray, Phys. Rev. B **13**, 4060 (1976).

[27] E. P. Elsukov, G. N. Konygin, V. A. Barinov, and E. V. Voronina, J. Phys.: Condens. Matter **4**, 7597 (1992).

[28] J. Kudrnovsky, N. E. Christensen, and O. K. Andersen, Phys. Rev. B **43**, 5924 (1991).

[29] N. G. Zamkova, V. S. Zhandun, I. S. Sandalov, and S. G. Ovchinnikov, J. Alloys Compd. **695**, 1213 (2017).

[30] J. Kanamori, Prog. Theor. Phys. **30**, 275 (1963).

[31] H. J. Monkhorst and J. D. Pack, Phys. Rev. B **13**, 5188 (1976).

[32] G. Kresse and J. Furthmuller, Comput. Mater. Sci. **6**, 15 (1996); Phys. Rev. B **54** 11169 (1996).

[33] P. E. Blochl, Phys. Rev. B **50**, 17953 (1994); G. Kresse and D. Joubert, *ibid.* **59**, 1758 (1999).

[34] J. P. Perdew, K. Burke, and M. Ernzerhof, Phys. Rev. Lett. **77**, 3865 (1996); **78**, 1396 (1997).

[35] P. Villars and L. D. Calvert, *Pearson's Handbook of Crystallographic Data for Intermetallic Phases* (American Society for Metals, Materials Park, OH, 1985).

[36] S. Eisebitt, J.-E. Rubensson, M. Nicodemus, T. Boske, S. Blugel, W. Eberhardt, K. Radermacher, S. Mantl, and G. Bihlmayer, Phys. Rev. B **50**, 18330 (1994).

[37] R. Girlanda, E. Piparo, and A. Balzarotti, J. Appl. Phys. **76**, 2837 (1994).

[38] E. G. Moroni, W. Wolf, J. Hafner, and R. Podloucky, Phys. Rev. B **59**, 12860 (1999).

[39] I. Sandalov, N. Zamkova, V. Zhandun, I. Tarasov, S. Varnakov, I. Yakovlev, L. Solovyov, and S. Ovchinnikov, Phys. Rev B **92**, 205129 (2015).

[40] D. A. Rowlands, Rep. Prog. Phys. **72**, 086501 (2009).